Science
AAAS

Supplementary Materials for

Control of reactive collisions by quantum interference

Hyungmok Son *et al*.

Corresponding author: Hyungmok Son, hson@g.harvard.edu

Science **375**, 1006 (2022)
DOI: 10.1126/science.abl7257

The PDF file includes:

Supplementary Text

Loss rate measurement & density calibration

In the main article, we provided the basic concept of how we acquired loss rates for Na+NaLi collisions, by comparing the initial loss rates with and without sodium atoms. For better accuracy, we evaluated the whole decay curve of molecules taking the time-dependent sodium numbers and particle temperatures into account, by numerically solving the differential equations:

$$\dot{N}_{\text{NaLi}} = -(K/V_{\text{ov}})N_{\text{Na}}N_{\text{NaLi}} - (\beta/V_{\text{eff}})N_{\text{NaLi}}^2 \tag{S1}$$

$$\dot{N}_{\text{Na}} = -(K/V_{\text{ov}})N_{\text{NaLi}}N_{\text{Na}}, \tag{S2}$$

where N_i represents the effective number of particles of type i per pancake, V_{ov} is the volume of the regime where atoms overlap with the more tightly confined molecules, and V_{eff} is the mean volume of molecules. β is the two-body molecular loss rate coefficient and K is the loss rate coefficient for the collisions of Na+NaLi pairs.

To determine rate coefficients from equations Eq. (S1) and Eq. (S2) requires accurate knowledge of the volumes V_{eff} and V_{ov} for a single pancake and knowledge of the effective particle number per pancake, which is the weighted average over the entire ensemble of pancakes. We will discuss this below.

In our primary calibration, however, we avoided this complication by comparing the decay of the mixture in the stretched spin state around the Feshbach resonance to that in a non-stretched spin state where the rate coefficient K is reliably predicted to be the s-wave universal loss rate coefficient. For this, we prepared sodium atoms in the lowest hyperfine state ($|F, m_F\rangle = |1, 1\rangle$ at the low field) and molecules are in their upper spin stretched state. For these initial states, the Na+NaLi system has a 50% doublet character. The doublet potential at short range is highly reactive due to exothermic nature and the collisional loss is predicted to

occur at the s-wave universal rate (33). In other words, we compared the decay of samples in the spin stretched and non-stretched states with the same initial densities, i.e. with the same effective particle numbers and the same volumes V_{eff} and V_{ov}. The only difference was the rate coefficient K, and by comparing the two decay curves, we obtained an accurate value for the ratio of the two K coefficients without an accurate model for the volumes and the ensemble of pancakes. Multiple calibration measurements with the non-stretched spin state mixture suggest a total uncertainty of the density calibration of $\sim 40\%$.

We have validated the assumption of the universal decay of the mixture in the non-stretched state by carrying out an independent absolute calibration. In this calibration, we obtained the effective particle numbers from the measured numbers of atoms and molecules and their distributions over pancakes, and the overlap volume using a full anharmonic model of the trapping potential and measured temperatures. For the accurate estimation, we had to sum the decay curves over the ensemble of pancakes, or alternatively, calculate the effective particle numbers per pancake and consider an effective decay curve using them. Since the observed axial profiles over pancakes of both Na and NaLi followed Gaussian fits with widths $\sigma_{\text{NaLi}}=450(60)\mu$m and $\sigma_{\text{Na}}=630(60)\mu$m, we assumed a Gaussian distribution of the particle number per pancake. The particle numbers in the central pancakes, N^0_{Na} and N^0_{NaLi}, are related to the total particle numbers $N^{\text{tot}}_{\text{Na}}=\sqrt{2\pi}\sigma_{\text{Na}}N^0_{\text{Na}}/a$ and $N^{\text{tot}}_{\text{NaLi}}=\sqrt{2\pi}\sigma_{\text{NaLi}}N^0_{\text{NaLi}}/a$ where the lattice constant, $a=\lambda/2$ and $\lambda=1,596$ nm. As the averages weighted over a Gaussian, the effective particle numbers per pancake in Eq. (S1) become $N^{\text{eff}}_{\text{NaLi}}=N^0_{\text{NaLi}}/\sqrt{2}$ and $N^{\text{eff}}_{\text{Na}}=N^0_{\text{Na}}(\sigma_{ov}/\sigma_{\text{NaLi}})$, where $1/\sigma^2_{\text{ov}}=1/\sigma^2_{\text{Na}}+1/\sigma^2_{\text{NaLi}}$. In Eq. (S2), the effective particle numbers are $N^{\text{eff}}_{\text{Na}}=N^0_{\text{Na}}/\sqrt{2}$ and $N^{\text{eff}}_{\text{NaLi}}=N^0_{\text{NaLi}}(\sigma_{\text{ov}}/\sigma_{\text{Na}})$.

We now discuss the volumes V_{eff} and V_{ov} in Eqs. (S1) and (S2). Assuming a harmonic trap, one obtains $V_{\text{eff}} = \bar{\omega}^{-3}_{\text{NaLi}}(4\pi k_B T_{\text{NaLi}}/m_{\text{NaLi}})^{3/2}$ and $V_{\text{ov}}=(N_{\text{Na}}N_{\text{NaLi}})/(\int dV n_{\text{Na}}n_{\text{NaLi}}) = \bar{\omega}^{-3}_{\text{Na}}\left[(2\pi k_B T_{\text{Na}}/m_{\text{Na}})\left(1+(\alpha_{\text{Na}}/\alpha_{\text{NaLi}})(T_{\text{NaLi}}/T_{\text{Na}})\right)\right]^{\frac{3}{2}}$ where the geometric mean of the sodium

trap frequencies, $\bar{\omega}_{\mathrm{Na}}=(\omega_x\omega_y\omega_z)^{1/3}=2\pi\times(325\cdot460\cdot45000)^{1/3}$ Hz and the polarizability ratio, $\alpha_{\mathrm{NaLi}}/\alpha_{\mathrm{Na}} = (m\omega^2)_{\mathrm{NaLi}}/(m\omega^2)_{\mathrm{Na}} = 2.8(4)$.

However, the confinement in each pancake is strongly anharmonic . In our model, we use the actual beam geometry of a 1D lattice trap with a retro-reflected beam displaced by 2 mm (which is $\sim60\%$ of the Rayleigh range) and 43% power relative to the incoming beam. Both beams are linearly polarized and have the same beam waist of 43 μm. The trap depth is calculated from the measured trap frequencies. In the local density approximation, we obtain

$$1/V_{\mathrm{ov}} = \frac{\int dV e^{-\beta_{\mathrm{Na}}U_{\mathrm{Na}}(r,z)} e^{-\beta_{\mathrm{NaLi}}U_{\mathrm{NaLi}}(r,z)}}{[\int dV e^{-\beta_{\mathrm{Na}}U_{\mathrm{Na}}(r,z)}][\int dV e^{-\beta_{\mathrm{NaLi}}U_{\mathrm{NaLi}}(r,z)}]} \tag{S3}$$

where r is the radial coordinate, z is the axial coordinate along the beam direction, $\beta_i = (k_B T_i)^{-1}$, and $U_i(r,z)$ is the potential of a single lattice site for the particle i. The integration limits in both coordinates are determined by the equipotential contour of the local maximum formed by gravity that tilts the trap in the y-direction. We find that the harmonic overlap volume is smaller than the anharmonic volume by a factor of 1.8.

Using this model and calibration, we experimentally measured the absolute loss rate for the mixture in the non-stretched spin state to be 30% lower than the universal limit, which agrees with the prediction of universality within the experimental uncertainty of $\sim40\%$.

The validity of the anharmonic model is experimentally cross-checked by observing cross-dimensional thermalization which occurs with a cross section well known via the s-wave scattering length of sodium atoms (*52*), including the 2D correction of the elastic scattering rate (*38*). For this, V_{eff} is determined from the anharmonic trapping potential as

$$1/V_{\mathrm{eff}} = \frac{\int dV \mathrm{e}^{-2\beta_{\mathrm{Na}}U_{\mathrm{Na}}(r,z)}}{[\int dV \mathrm{e}^{-\beta_{\mathrm{Na}}U_{\mathrm{Na}}(r,z)}]^2} \tag{S4}$$

We find that the observed thermalization rate differs from the model prediction by $\sim10\%$, which is within the uncertainty of the thermalization measurement, $\sim15\%$.

When we use the same model for the trapping potential to obtain the two-body molecular loss rate coefficient, we find a factor of two discrepancy with the expected p-wave universal limit (*53*). This is most likely due to a non-equilibrium distribution of molecules over the different "pancakes" due to the formation process.

In summary, in the main paper, we have eliminated the need for absolute values of the overlap density $N_{\mathrm{Na}}^{\mathrm{eff}}/V_{\mathrm{ov}}$ by comparing loss rates around the Feshbach resonances to the loss rate of the mixture in the non-stretched spin state, which was predicted to be universal. We have validated this prediction by the calibration procedure and modeling described here. In other words, if we had not used the comparison with the non-stretched systems, we would have obtained the same results within the (now larger) uncertainties.

The loss rate coefficients reported here are somewhat different from previous values in Ref. *(30)* where the anharmonicity in the trapping potential and the polarization purity of the absorption imaging light were not fully considered.

Typical particle numbers $\&$ decay of sodium atoms

The typical particle numbers per pancake are 320 and 30 for Na and NaLi, respectively. With the typical statistical uncertainty of the particle number, $\sim 13\%$, the decay of the sodium number is insignificant and we can treat the number as constant during the hold time.

However, near the peak of the strong resonance, the molecular signal depletes quickly while we wait for the field to fully settle after ramping it. Thus, we typically work in the regime where $N_{\mathrm{Na}}/N_{\mathrm{NaLi}} = 125/23 \approx 5$. In this case, we find decay curves of both sodium atoms and molecules fit well to the analytic solution of Eq. (S1) and (S2) by ignoring the molecular two-body loss term which is two orders of magnitude smaller than the atom-molecule term. In this regime, the numerical solution of Eq. (S1) and (S2) agrees well with the analytic solution: $N_{\mathrm{Na}}(t) = -\mathrm{D}/(e^{-\mathrm{D}\Gamma t}/\mathrm{C} - 1), N_{\mathrm{NaLi}}(t) = \mathrm{D}/(\mathrm{C}e^{\mathrm{D}\Gamma t} - 1)$, where Γ is the loss rate

and $\mathrm{C} = N_{\mathrm{Na}}(0)/N_{\mathrm{NaLi}}(0), \mathrm{D} = N_{\mathrm{Na}}(0) - N_{\mathrm{NaLi}}(0)$. $N(0)$ is the initial particle number. When $D \approx N_{\mathrm{Na}}(0)$, the sodium number is approximately constant, and we find the decay curve of molecules fits well to a simple exponential function, $N_{\mathrm{NaLi}}(t) \approx N_{\mathrm{NaLi}}(0)e^{-\Gamma t}$.

Magnetic field inhomogeneity

After a mixture of molecules and atoms is initially prepared at 745 G, the bias field is ramped to the target value in 15 ms. Due to eddy currents, an extra hold time of 15 ms or more was added to allow the bias field to fully settle. Due to magnetic field curvature, the sample experiences a magnetic field inhomogeneity of $\lesssim 80$ mG near 1000 G. This upper bound is inferred from the narrowness of an RF spin-flip transition of sodium atoms.

Temperature of Na and NaLi Inelastic losses occur predominantly at the highest densities and lead to increase in temperature, sometimes called anti-evaporation. Near the peak of the strong resonance, molecules heat up before we start acquiring a decay curve. We observe that within ± 2.5 G around the peak, the molecule temperature is ~ 1.9 μK while the temperature of sodium atoms is at ~ 1.6 μK, due to the large imbalance of particle numbers. This gives the temperature associated with relative radial motion, $T_{\mathrm{rel}} = \mu(T_{\mathrm{Na}}/m_{\mathrm{Na}} + T_{\mathrm{mol}}/m_{\mathrm{mol}}) = 1.73(15)$ μK near the peak. Compared to the temperature away from the peak $T_{\mathrm{rel}} \sim 1.55$ μK, this is about 12% higher, and with the increased temperature, the fit result is still the same within the fit uncertainty. Further heating during the decay curve measurement is not observed.

Verification of two-body loss mechanism

We have treated the loss dynamics as purely two-body collisions. Because the scattering length near the peak gets very large, we checked that the decay is still dominated by two-body decay. Fig. S1 shows indeed a linear dependency of the loss rate of molecules on the overlap density.

It is acquired near the peak of the strong resonance, at 981 G where $\mathrm{Re}[\tilde{a}] = -940\ a_0$. The blue dotted line is a linear fit ($\chi^2_{\mathrm{red}} = 0.3$) and the red line is a quadratic fit ($\chi^2_{\mathrm{red}} = 3.9$). This shows the observed losses have negligible contribution from three-body decay with $\mathrm{n}^2_{\mathrm{Na}}\mathrm{n}_{\mathrm{NaLi}}$ (n_i is the density of particle i). The inset shows a linear fit of $\ln(\mathrm{N}_{\mathrm{NaLi}}(t))$ with $\chi^2_{\mathrm{red}} = 0.3$. In comparison, a linear fit of $\mathrm{N}_{\mathrm{NaLi}}(t)^{-1}$, which would reflect three-body decay with $\mathrm{n}_{\mathrm{Na}}\mathrm{n}^2_{\mathrm{NaLi}}$, gives $\chi^2_{\mathrm{red}} = 4.1$ (not shown in the figure).

Mapping between Fabry-Perot model and threshold scattering formalism

In the main text, we have shown that the results of the multichannel quantum defect model in the threshold regime can be expressed by the Fabry-Perot contrast. Here we show how the multiple reflections are treated in a S matrix formalism.

The quantum reflection and transmission of the scattering wavefunction in the long-range regime are formulated in terms of $r^{io}(r^{oi})$ and $t^{io}(t^{oi})$, the amplitude reflection and transmission coefficients for the wave travelling inward (outward) respectively, as introduced in (*26,36,54*) In general, r^{oi} and r^{io} have different phases. The coefficient of the short-range reflection with loss is the short-range S-matrix, $S^c = \xi e^{i2\delta_s}$ where $\xi = (1-y)/(1+y)$ and y is the quantum-defect parameter, as given in (*26,55*). δ_s is the short-range phase shift with a finite range $0 \leq \delta_s < \pi$ (*26*).

The transmission through the total potential is obtained as the coherent sum of multiple reflection pathways in the range $R_{\mathrm{short}} < R < R_{\mathrm{long}}$ (*55*):

$$\begin{aligned} T &= I|\sqrt{1-\xi^2}t^{oi}(1 + r^{io}S^c + (r^{io}S^c)^2 + ...)|^2 \\ &= I|\sqrt{1-\xi^2}t^{oi}|^2(1 - r^{io}S^c)^{-1} \end{aligned} \tag{S5}$$

where I is the influx. Ref. (*36*) gives an analytic solution of the phase factors for the reflection coefficients. For s-wave collisions with vdW interaction, the phases of r^{oi} and r^{io} are π and

$-\pi/4$ respectively. This simplifies the transmission as follows:

$$T = I|t^{oi}|^2\left(\frac{|\sqrt{1-\xi^2}|^2}{|1-|r^{io}|\xi e^{i(2(\delta_s-\pi/8))}|^2}\right) \equiv I|t_2|^2 C \tag{S6}$$

This is identical to the transmission through two reflectors, given as Eq. (1) in the main article, with $|t_2| = |\sqrt{1-\xi^2}|$, $|r_1| = |r^{oi}| = |r^{io}|$, $\xi = |r_2|$. The negative round-trip phase $-\phi$ is twice the short-range phase shift $2\delta_s$ plus the phase shift due to the quantum reflection at long range $-\pi/4$ (i.e., $-\phi = 2\delta_s - \pi/4$).

Mapping of two-channel model to Breit-Wigner form

Scattering resonances are described by a complex scattering length $\tilde{a}$ which moves across a circle in the complex plane as the resonance is crossed (*27,43*). The most general resonance has six parameters (the two center coordinates and the radius of the circle, the position of the background on the circle, and the position/width of the resonance in magnetic field). Here we show that our two-channel model which has six parameters can be mapped to the standard Breit-Wigner form describing an isolated resonance. In contrast, the one-channel Fabry-Perot model has only five parameters since the position and radius of the circle are constrained and depend only on y and $\bar{a}$ (*11*).

The complex scattering length defined by the two-channel model with parameters ($B_{\rm res}, \Delta, y, q, \Gamma_{\rm b}, \bar{a}$) is given by:

$$\tilde{a}(B) = \bar{a}\left(s(B) + y\frac{1+(1-s(B))^2}{i+y(1-s(B))}\right) \equiv \alpha(B) - i\beta(B) \tag{S7}$$

The Feshbach resonance with a lossy bound state is described by:

$$s(B) = q\left(1 - \frac{\Delta}{B - B_{\rm res} - i\Gamma_{\rm b}/2}\right) \tag{S8}$$

We can re-write the two-channel model, Eq. (S7), in the usual Breit-Wigner form (*27*) in terms of the complex background scattering length $\tilde{a}_{\rm bg}$, the resonant scattering length, $\tilde{a}_{\rm res}$, the

resonance position, B^o_{res}, and the width, Γ_{inel}:

$$\begin{aligned}\tilde{a}(B) &= \tilde{a}_{\text{bg}} + \frac{\tilde{a}_{\text{res}}}{2(B - B^o_{\text{res}})/\Gamma_{\text{inel}} - i} \\ &\equiv \alpha(B) - i\beta(B)\end{aligned} \tag{S9}$$

The mapping between two parameter sets is as follows:

$$\begin{aligned}B^o_{\text{res}} &= B_{\text{res}} + \frac{qy^2\Delta(q-1)}{1+y^2(q-1)^2} \\ \Gamma_{\text{inel}} &= \Gamma_{\text{b}} + \frac{2yq\Delta}{1+y^2(q-1)^2} \equiv \Gamma_{\text{b}} + \Gamma_{\text{c}}\end{aligned}$$

$$\begin{aligned}\tilde{a}_{\text{bg}} &= \frac{y(2-q)+iq}{i+y(1-q)}\,\bar{a} \equiv \alpha_{\text{bg}} - i\beta_{\text{bg}} \\ \alpha_{\text{bg}} &= \frac{q+(q-2)(q-1)y^2}{1+(q-1)^2y^2}\,\bar{a} \\ \beta_{\text{bg}} &= \frac{(2+(q-2)q)y}{1+(q-1)^2y^2}\,\bar{a}\end{aligned} \tag{S10}$$

$$\begin{aligned}\tilde{a}_{\text{res}} &= \frac{2}{\Gamma_{\text{inel}}}\frac{(1-y^2)q\Delta}{(i+y(1-q))^2}\,\bar{a} \equiv \alpha_{\text{res}} - i\beta_{\text{res}} \\ \alpha_{\text{res}} &= \frac{-2q\Delta(1-y^2)(1-y^2(q-1)^2)}{(1+(q-1)^2y^2)[(1+(q-1)^2y^2)\Gamma_{\text{b}}+2qy\Delta]}\,\bar{a} \\ \beta_{\text{res}} &= \frac{4qy\Delta(q-1)(y^2-1)}{(1+(q-1)^2y^2)[(1+(q-1)^2y^2)\Gamma_{\text{b}}+2qy\Delta]}\,\bar{a}\end{aligned}$$

where the width of the resonance Γ_{inel} is the incoherent sum of two decay rates: the natural linewidth of the bound state, Γ_{b} and the width determined by the coupling strength between the scattering state and the bound state, Γ_{c}. Note that both width factors have units of magnetic field. The energy width is obtained by dividing by $\delta\mu$. Since the energy widths are positive definite, the signs of Γ_{b} and Γ_{c} are determined by the sign of $\delta\mu$. In our case, Γ_{b} and Γ_{c} are positive since $\delta\mu > 0$. When $\delta\mu < 0$, $\Gamma_{\text{b}} < 0$ by definition, and $\Gamma_{\text{c}} < 0$ since $q \cdot \Delta < 0$ (see Sign constraints for parameters q and Δ).

The imaginary part of the scattering length is given by:

$$\beta = \beta_{\text{bg}} + \frac{-\alpha_{\text{res}}(\Gamma_{\text{inel}}/2)^2 + \beta_{\text{res}}(\Gamma_{\text{inel}}/2)(B - B^o_{\text{res}})}{(B - B^o_{\text{res}})^2 + (\Gamma_{\text{inel}}/2)^2} \tag{S11}$$

It is straightforward to check that the peak height is $\beta = 1/y$ at $B{=}B_{\text{res}}$, as expected.

For $y \ll 1$, $q \sim 1$, and $\Gamma_{\text{inel}} \approx \Gamma_{\text{c}}$:

$$\beta(B) \approx \beta_{\text{bg}} + yq\Delta\left[\frac{q\Delta + 2(1-q)(B - B^o_{\text{res}})}{(B - B^o_{\text{res}})^2 + (yq\Delta)^2}\right]\bar{a} \tag{S12}$$

This shows that due to the second term in the numerator, $q > 1$ and $q < 1$ give different asymmetries in the lineshape.

In contrast, for $y \ll 1$, $q \sim 1$, and $\Gamma_{\text{inel}} \approx \Gamma_{\text{b}}$:

$$\beta(B) \approx \beta_{\text{bg}} + q\Delta\left[\frac{\Gamma_{\text{b}}/2 + 2y(1-q)(B - B^o_{\text{res}})}{(B - B^o_{\text{res}})^2 + (\Gamma_{\text{b}}/2)^2}\right]\bar{a} \tag{S13}$$

In this case, the asymmetry is small and the lineshape can be well-approximated by a Lorentzian.

Sign constraints for parameters q and Δ

By definition, q and $\delta\mu\Delta$ have the same sign (*2*) where $\delta\mu = \mu_{\text{Na+NaLi}} - \mu_{\text{bound}}$ is the relative magnetic moment between the entrance channel and the closed channel bound state. In our case, $\mu_{\text{Na+NaLi}} = 3\mu_{\text{B}}$ as the entrance channel is in the upper spin-stretched state where three electronic spins are aligned along the bias field direction. Thus, $\delta\mu = 4\mu_{\text{B}}(2\mu_{\text{B}}) > 0$, if the bound state we couple requires two(one) spins to flip. This constrains the signs of Δ and q to be the same, i.e. $q \cdot \Delta{>}0$. The observed asymmetry of the loss lineshape requires $q{>}1$, which implies $\Delta{>}0$.

Thermal averaging

At our temperature, $k_B T{<}\hbar\omega_{ax}$, the scattering is dominated by the axial motional ground-state channel (*38*) and the saturation factor does not depend on temperature $f(k) = (1 +$

$(\sqrt{\pi}/l_o)^2|l|^2|\tilde{a}|^2 + 2(\sqrt{\pi}/l_o)|l|^2\beta)^{-1}$. However, the logarithmic correction factor, l=$|(1 + (\tilde{a}/\sqrt{\pi}l_o)\ln(B\hbar\omega_{ax}/\pi\epsilon))|^{-2}$ (where ϵ=$\hbar^2q^2/2\mu$, B≈0.915, and l_o=$\sqrt{\hbar/\mu\omega_{ax}}$) depends on the radial momentum q. In the main article, we used the mean thermal energy k_BT for the radial relative kinetic energy ϵ. A more accurate way is to perform a thermal average.

The thermal average for the loss rate ratio $r(B) = f(k)l(\beta/\bar{a})$ is given by:

$$\langle r(B)\rangle = \frac{\beta f(k)}{\bar{a}}\frac{\lambda}{Z}\left(\int_0^\infty dq\ 2\pi q\ l(q)e^{\frac{-\hbar^2q^2}{2\mu k_BT}}\right) \tag{S14}$$

where $Z = \mu k_BT/\hbar^2$, and $\lambda = \sqrt{1 - e^{-2\hbar\omega_{\rm ax}/k_BT}}$ is the normalization constant for the average over the axial direction (*56*). At our temperature T∼1.55 μK, the thermal average effect shifts the peak loss position by ∼0.3 G, almost canceling the shift caused by the mean thermal energy, ϵ=k_BT. Fit parameters except $B_{\rm res}$ agree with the result without the thermal average within the fit uncertainties.

Ratio of elastic to inelastic collision rates

Figure S2 shows the good-to-bad collision ratio, γ=$k(\alpha^2 + \beta^2)/\beta$. It is maximized away from the Feshbach resonance, since near the resonance, the increase in the elastic scattering rate, which is proportional to $(\alpha^2+\beta^2)$, is less than the increase in the inelastic scattering rate, which is proportional to β/k. The minimum of γ is not at the resonance but at 1006.9 G where the real part of the scattering length, α crosses zero and the imaginary part, β is close to it background value. Note that this plot uses only the parameters obtained from the analysis of the resonance at 978 G. In the previous work Ref. *(30)*, we demonstrated sympathetic cooling of NaLi molecules with Na atoms near 745 G and measured a higher ratio of good-to-bad collisions of about 100. This discrepancy is presumed to be caused by contributions from other Feshbach resonances and is the subject of future studies. Also, in Ref. *(30)* we measured elastic collisions directly by observing thermalization, whereas here we inferred an elastic collision rate only from the

analysis of observed inelastic rates.

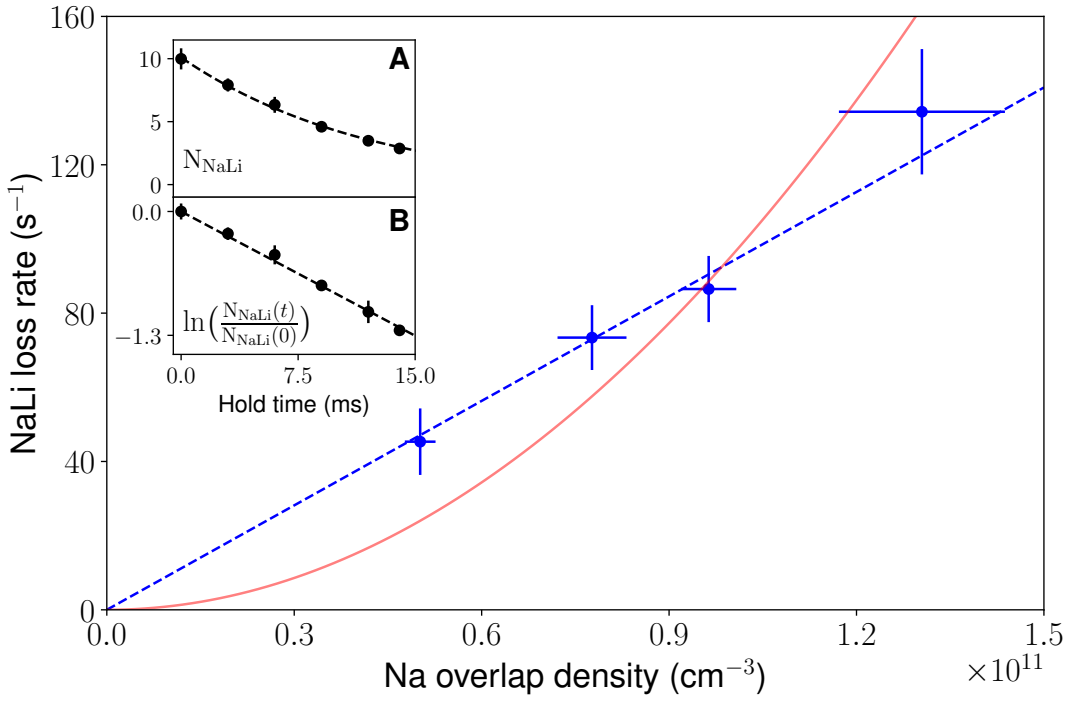

Fig. S1.

Verification of two-body loss mechanism. The loss rate of molecules is shown as a function of the overlap density at 978.7 G, near the peak of the strong resonance and shows a linear dependence (blue dashed line). The red line is a quadratic fit. The error bar of the y-data is one standard deviation. The error bar of the x-data is one standard error of the mean. In this figure, we are not including the calibration uncertainty for the Na density. The inset (**A**) shows a decay curve of molecules with overlap density $9.6(4) \times 10^{10}$ cm^{-3}, and (**B**) shows a linearized decay curve with a linearized exponential fit at the same overlap density.

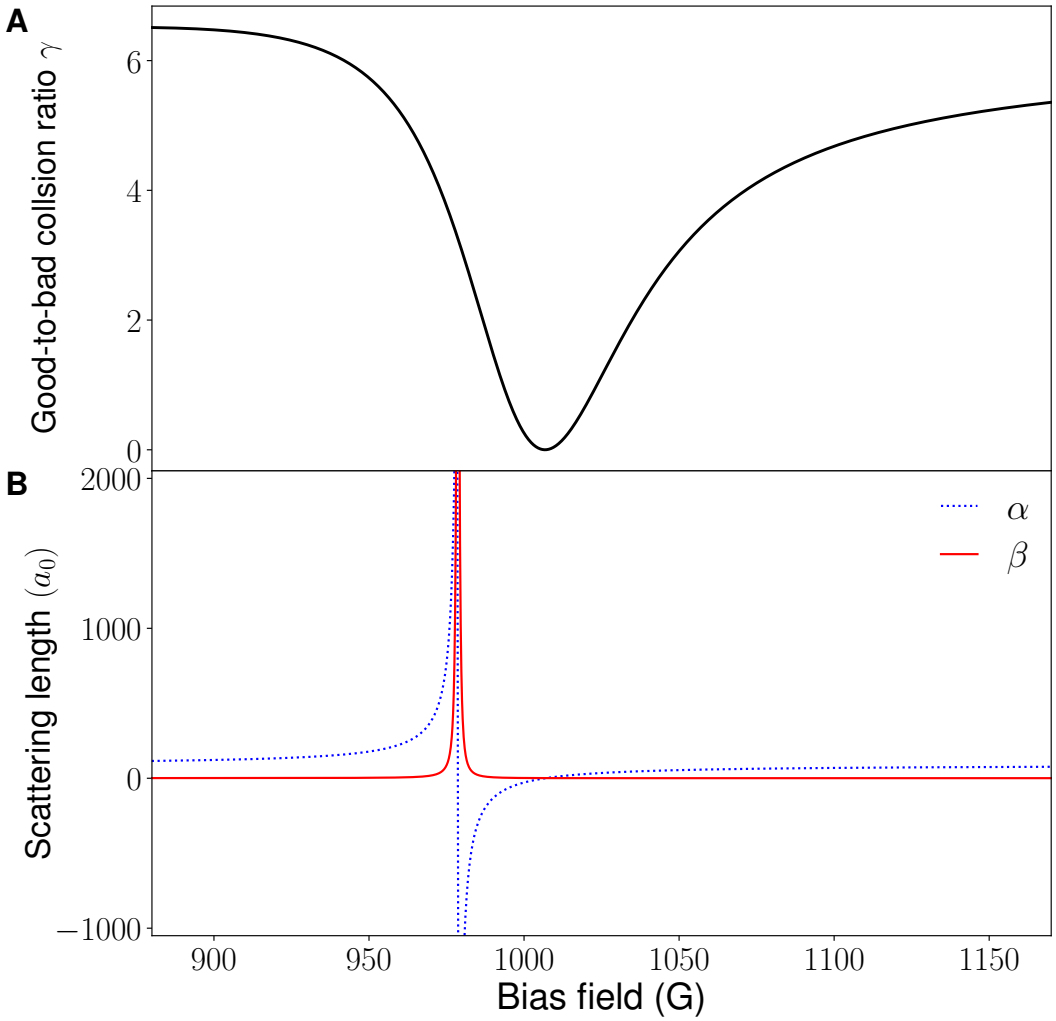

Fig. S2.

Ratio of elastic to inelastic collision rates near the strong resonance. (**A**) The good-to-bad collision ratio, $\gamma{=}k(\alpha^2 + \beta^2)/\beta$ as a function of the bias field, where α and β are the real and and imaginary parts of the complex scattering length respectively, the relative wavevector $k = \mu v_{\text{rel}}/\hbar$ and $v_{\text{rel}} = \sqrt{8k_B T/\mu\pi}$ (μ: the reduced mass between NaLi and Na, $T = 1.55\mu$K). (**B**) α and β around the strong resonance at 978 G. Note that the effect of the small resonance at 1030 G has not been considered in the calculation of γ.

References and Notes

1. S. Inouye, M. R. Andrews, J. Stenger, H.-J. Miesner, D. M. Stamper-Kurn, W. Ketterle, Observation of feshbach resonances in a Bose–Einstein condensate. *Nature* **392**, 151–154 (1998). doi:10.1038/32354

2. C. Chin, R. Grimm, P. Julienne, E. Tiesinga, Feshbach resonances in ultracold gases. *Rev. Mod. Phys.* **82**, 1225–1286 (2010). doi:10.1103/RevModPhys.82.1225

3. A. B. Henson, S. Gersten, Y. Shagam, J. Narevicius, E. Narevicius, Observation of resonances in Penning ionization reactions at sub-kelvin temperatures in merged beams. *Science* **338**, 234–238 (2012). doi:10.1126/science.1229141 Medline

4. T. de Jongh, M. Besemer, Q. Shuai, T. Karman, A. van der Avoird, G. C. Groenenboom, S. Y. T. van de Meerakker, Imaging the onset of the resonance regime in low-energy NO-He collisions. *Science* **368**, 626–630 (2020). doi:10.1126/science.aba3990 Medline

5. L. D. Carr, D. DeMille, R. V. Krems, J. Ye, Cold and ultracold molecules: Science, technology and applications. *New J. Phys.* **11**, 055049 (2009). doi:10.1088/1367-2630/11/5/055049

6. Y. Liu, M.-G. Hu, M. A. Nichols, D. Yang, D. Xie, H. Guo, K.-K. Ni, Precision test of statistical dynamics with state-to-state ultracold chemistry. *Nature* **593**, 379–384 (2021). doi:10.1038/s41586-021-03459-6 Medline

7. M. Mayle, B. P. Ruzic, J. L. Bohn, Statistical aspects of ultracold resonant scattering. *Phys. Rev. A* **85**, 062712 (2012). doi:10.1103/PhysRevA.85.062712

8. A. Christianen, M. W. Zwierlein, G. C. Groenenboom, T. Karman, Photoinduced two-body loss of ultracold molecules. *Phys. Rev. Lett.* **123**, 123402 (2019). doi:10.1103/PhysRevLett.123.123402 Medline

9. P. D. Gregory, J. A. Blackmore, S. L. Bromley, S. L. Cornish, Loss of ultracold $^{87}Rb^{133}Cs$ molecules via optical excitation of long-lived two-body collision complexes. *Phys. Rev. Lett.* **124**, 163402 (2020). doi:10.1103/PhysRevLett.124.163402 Medline

10. Y. Liu, M.-G. Hu, M. A. Nichols, D. D. Grimes, T. Karman, H. Guo, K.-K. Ni, Photo-excitation of long-lived transient intermediates in ultracold reactions. *Nat. Phys.* **16**, 1132–1136 (2020). doi:10.1038/s41567-020-0968-8

11. Z. Idziaszek, P. S. Julienne, Universal rate constants for reactive collisions of ultracold molecules. *Phys. Rev. Lett.* **104**, 113202 (2010). doi:10.1103/PhysRevLett.104.113202 Medline

12. R. V. Krems, Molecules near absolute zero and external field control of atomic and molecular dynamics. *Int. Rev. Phys. Chem.* **24**, 99–118 (2005). doi:10.1080/01442350500167161

13. M. T. Bell, T. P. Softley, Ultracold molecules and ultracold chemistry. *Mol. Phys.* **107**, 99–132 (2009). doi:10.1080/00268970902724955

14. S. Ospelkaus, K.-K. Ni, D. Wang, M. H. G. de Miranda, B. Neyenhuis, G. Quéméner, P. S. Julienne, J. L. Bohn, D. S. Jin, J. Ye, Quantum-state controlled chemical reactions of

ultracold potassium-rubidium molecules. *Science* **327**, 853–857 (2010). doi:10.1126/science.1184121 Medline

15. J. W. Park, S. A. Will, M. W. Zwierlein, Ultracold dipolar gas of fermionic $^{23}Na^{40}K$ molecules in their absolute ground state. *Phys. Rev. Lett.* **114**, 205302 (2015). doi:10.1103/PhysRevLett.114.205302 Medline

16. X. Ye, M. Guo, M. L. González-Martínez, G. Quéméner, D. Wang, Collisions of ultracold $^{23}Na^{87}Rb$ molecules with controlled chemical reactivities. *Sci. Adv.* **4**, eaaq0083 (2018). doi:10.1126/sciadv.aaq0083 Medline

17. P. D. Gregory, M. D. Frye, J. A. Blackmore, E. M. Bridge, R. Sawant, J. M. Hutson, S. L. Cornish, Sticky collisions of ultracold RbCs molecules. *Nat. Commun.* **10**, 3104 (2019). doi:10.1038/s41467-019-11033-y Medline

18. T. Takekoshi, L. Reichsöllner, A. Schindewolf, J. M. Hutson, C. R. Le Sueur, O. Dulieu, F. Ferlaino, R. Grimm, H.-C. Nägerl, Ultracold dense samples of dipolar RbCs molecules in the rovibrational and hyperfine ground state. *Phys. Rev. Lett.* **113**, 205301 (2014). doi:10.1103/PhysRevLett.113.205301 Medline

19. L. W. Cheuk, L. Anderegg, Y. Bao, S. Burchesky, S. S. Yu, W. Ketterle, K.-K. Ni, J. M. Doyle, Observation of collisions between two ultracold ground-state CaF molecules. *Phys. Rev. Lett.* **125**, 043401 (2020). doi:10.1103/PhysRevLett.125.043401 Medline

20. B. Drews, M. Deiß, K. Jachymski, Z. Idziaszek, J. Hecker Denschlag, Inelastic collisions of ultracold triplet Rb_2 molecules in the rovibrational ground state. *Nat. Commun.* **8**, 14854 (2017). doi:10.1038/ncomms14854 Medline

21. G. Polovy, E. Frieling, D. Uhland, J. Schmidt, K. W. Madison, Quantum-state-dependent chemistry of ultracold $^6Li_2$ dimers. *Phys. Rev. A* **102**, 013310 (2020). doi:10.1103/PhysRevA.102.013310

22. E. R. Hudson, N. B. Gilfoy, S. Kotochigova, J. M. Sage, D. DeMille, Inelastic collisions of ultracold heteronuclear molecules in an optical trap. *Phys. Rev. Lett.* **100**, 203201 (2008). doi:10.1103/PhysRevLett.100.203201 Medline

23. N. Zahzam, T. Vogt, M. Mudrich, D. Comparat, P. Pillet, Atom-molecule collisions in an optically trapped gas. *Phys. Rev. Lett.* **96**, 023202 (2006). doi:10.1103/PhysRevLett.96.023202 Medline

24. P. Staanum, S. D. Kraft, J. Lange, R. Wester, M. Weidemüller, Experimental investigation of ultracold atom-molecule collisions. *Phys. Rev. Lett.* **96**, 023201 (2006). doi:10.1103/PhysRevLett.96.023201 Medline

25. J. Deiglmayr, M. Repp, A. Grochola, O. Dulieu, R. Wester, M. Weidemüller, Dipolar effects and collisions in an ultracold gas of LiCs molecules. *J. Phys. Conf. Ser.* **264**, 012014 (2011). doi:10.1088/1742-6596/264/1/012014

26. M. D. Frye, P. S. Julienne, J. M. Hutson, Cold atomic and molecular collisions: Approaching the universal loss regime. *New J. Phys.* **17**, 045019 (2015). doi:10.1088/1367-2630/17/4/045019

27. J. M. Hutson, Feshbach resonances in ultracold atomic and molecular collisions: Threshold behaviour and suppression of poles in scattering lengths. *New J. Phys.* **9**, 152 (2007). doi:10.1088/1367-2630/9/5/152

28. X.-Y. Wang, M. D. Frye, Z. Su, J. Cao, L. Liu, D.-C. Zhang, H. Yang, J. M. Hutson, B. Zhao, C.-L. Bai, J.-W. Pan, Magnetic Feshbach resonances in collisions of $^{23}Na^{40}K$ with ^{40}K. *New J. Phys.* **23**, 115010 (2021). doi:10.1088/1367-2630/ac3318

29. H. Yang, X.-Y. Wang, Z. Su, J. Cao, D.-C. Zhang, J. Rui, B. Zhao, C.-L. Bai, J.-W. Pan, Evidence for association of triatomic molecule in ultracold $^{23}Na^{40}K$ and ^{40}K mixture. arXiv:2104.11424 [physics.atom-ph] (2021).

30. H. Son, J. J. Park, W. Ketterle, A. O. Jamison, Collisional cooling of ultracold molecules. *Nature* **580**, 197–200 (2020). doi:10.1038/s41586-020-2141-z Medline

31. T. M. Rvachov, H. Son, A. T. Sommer, S. Ebadi, J. J. Park, M. W. Zwierlein, W. Ketterle, A. O. Jamison, Long-lived ultracold molecules with electric and magnetic dipole moments. *Phys. Rev. Lett.* **119**, 143001 (2017). doi:10.1103/PhysRevLett.119.143001 Medline

32. B. Gao, Universal model for exoergic bimolecular reactions and inelastic processes. *Phys. Rev. Lett.* **105**, 263203 (2010). doi:10.1103/PhysRevLett.105.263203 Medline

33. R. Hermsmeier, J. Kłos, S. Kotochigova, T. V. Tscherbul, Quantum spin state selectivity and magnetic tuning of ultracold chemical reactions of triplet alkali-metal dimers with alkali-metal atoms. *Phys. Rev. Lett.* **127**, 103402 (2021). doi:10.1103/PhysRevLett.127.103402 Medline

34. G. F. Gribakin, V. V. Flambaum, Calculation of the scattering length in atomic collisions using the semiclassical approximation. *Phys. Rev. A* **48**, 546–553 (1993). doi:10.1103/PhysRevA.48.546 Medline

35. This expression is equivalent to $\tan(\phi/2) = 1/(1-s)$, which is also given in (*26*).

36. Y.-P. Bai, J.-L. Li, G.-R. Wang, S.-L. Cong, Model for investigating quantum reflection and quantum coherence in ultracold molecular collisions. *Phys. Rev. A* **100**, 012705 (2019). doi:10.1103/PhysRevA.100.012705

37. Y. Xie, H. Zhao, Y. Wang, Y. Huang, T. Wang, X. Xu, C. Xiao, Z. Sun, D. H. Zhang, X. Yang, Quantum interference in H + HD → H_2 + D between direct abstraction and roaming insertion pathways. *Science* **368**, 767–771 (2020). doi:10.1126/science.abb1564 Medline

38. D. S. Petrov, G. V. Shlyapnikov, Interatomic collisions in a tightly confined Bose gas. *Phys. Rev. A* **64**, 012706 (2001). doi:10.1103/PhysRevA.64.012706

39. Z. Idziaszek, K. Jachymski, P. S. Julienne, Reactive collisions in confined geometries. *New J. Phys.* **17**, 035007 (2015). doi:10.1088/1367-2630/17/3/035007

40. Although the relative motion is no longer a simple harmonic oscillator, the expression for ω_{ax} provides the correct kinetic energy $\hbar\omega_{ax}/4$ of the relative motion.

41. In (*50*), Yang *et al*. mention a resonant loss rate two to three times the universal limit. However, this is based on an estimate for the universal limit and an unspecified density

calibration. Our weak resonance shows that it is easily possible to observe Feshbach resonances that do not exceed the universal limit.

42. J. M. Hutson, M. Beyene, M. L. González-Martínez, Dramatic reductions in inelastic cross sections for ultracold collisions near Feshbach resonances. *Phys. Rev. Lett.* **103**, 163201 (2009). doi:10.1103/PhysRevLett.103.163201 Medline

43. R. A. Rowlands, M. L. Gonzalez-Martinez, J. M. Hutson, Ultracold collisions in magnetic fields: reducing inelastic cross sections near Feshbach resonances. arXiv:0707.4397 [physics.chem-ph] (2007).

44. L. Anderegg, S. Burchesky, Y. Bao, S. S. Yu, T. Karman, E. Chae, K.-K. Ni, W. Ketterle, J. M. Doyle, Observation of microwave shielding of ultracold molecules. *Science* **373**, 779–782 (2021). doi:10.1126/science.abg9502 Medline

45. S. Jurgilas, A. Chakraborty, C. J. H. Rich, L. Caldwell, H. J. Williams, N. J. Fitch, B. E. Sauer, M. D. Frye, J. M. Hutson, M. R. Tarbutt, Collisions between ultracold molecules and atoms in a magnetic trap. *Phys. Rev. Lett.* **126**, 153401 (2021). doi:10.1103/PhysRevLett.126.153401 Medline

46. K. K. Voges, P. Gersema, M. Meyer Zum Alten Borgloh, T. A. Schulze, T. Hartmann, A. Zenesini, S. Ospelkaus, Ultracold gas of bosonic $^{23}Na^{39}K$ ground-state molecules. *Phys. Rev. Lett.* **125**, 083401 (2020). doi:10.1103/PhysRevLett.125.083401 Medline

47. T. T. Wang, M.-S. Heo, T. M. Rvachov, D. A. Cotta, W. Ketterle, Deviation from universality in collisions of ultracold $^{6}Li_2$ molecules. *Phys. Rev. Lett.* **110**, 173203 (2013). doi:10.1103/PhysRevLett.110.173203 Medline

48. Z. Z. Yan, J. W. Park, Y. Ni, H. Loh, S. Will, T. Karman, M. Zwierlein, Resonant dipolar collisions of ultracold molecules induced by microwave dressing. *Phys. Rev. Lett.* **125**, 063401 (2020). doi:10.1103/PhysRevLett.125.063401 Medline

49. K. Matsuda, L. De Marco, J.-R. Li, W. G. Tobias, G. Valtolina, G. Quéméner, J. Ye, Resonant collisional shielding of reactive molecules using electric fields. *Science* **370**, 1324–1327 (2020). doi:10.1126/science.abe7370 Medline

50. H. Yang, D.-C. Zhang, L. Liu, Y.-X. Liu, J. Nan, B. Zhao, J.-W. Pan, Observation of magnetically tunable Feshbach resonances in ultracold $^{23}Na^{40}K + ^{40}K$ collisions. *Science* **363**, 261–264 (2019). doi:10.1126/science.aau5322 Medline

51. H. Son, J. J. Park, Y.-K. Lu, A. O. Jamison, T. Karman, W. Ketterle, Data of: Control of reactive collisions by quantum interference, version 1, Zenodo (2021); https://doi.org/10.5281/zenodo.5797536.

52. E. Tiesinga, C. J. Williams, P. S. Julienne, K. M. Jones, P. D. Lett, W. D. Phillips, A spectroscopic determination of scattering lengths for sodium atom collisions. *J. Res. Natl. Inst. Stand. Technol.* **101**, 505–520 (1996). doi:10.6028/jres.101.051 Medline

53. The p-wave universal rate of the molecular loss is calculated with the sum of the C_6 coefficients for the atomic pairs that constitute the collision partners, using values from (*57*).

54. B. Gao, General form of the quantum-defect theory for $-1/r^{\alpha}$ type of potentials with $\alpha > 2$. *Phys. Rev. A* **78**, 012702 (2008). doi:10.1103/PhysRevA.78.012702

55. Y.-P. Bai, J.-L. Li, G.-R. Wang, Z.-B. Chen, B.-W. Si, S.-L. Cong, Simple analytical model for high-partial-wave ultracold molecular collisions. *Phys. Rev. A* **101**, 063605 (2020). doi:10.1103/PhysRevA.101.063605

56. P. Naidon, P. S. Julienne, Optical Feshbach resonances of alkaline-earth-metal atoms in a one- or two-dimensional optical lattice. *Phys. Rev. A* **74**, 062713 (2006). doi:10.1103/PhysRevA.74.062713

57. A. Derevianko, J. F. Babb, A. Dalgarno, High-precision calculations of van der waals coefficients for heteronuclear alkali-metal dimers. *Phys. Rev. A* **63**, 052704 (2001). doi:10.1103/PhysRevA.63.052704